DOI: 10.1002/adma.200702209

Rational Synthesis Pathway for Ordered Mesoporous Carbon with Controllable 30- to 100-Angstrom Pores**

By Hyung Ik Lee, Jin Hoe Kim, Dae Jong You, Ji Eun Lee, Ji Man Kim, Wha-Seung Ahn, Chanho Pak,* Sang Hoon Joo, Hyuk Chang,* and *Doyoung Seung*

Since the first report on the successful synthesis of ordered mesoporous carbon (OMC) using a mesoporous silica template,[1] OMCs have been of great interest due to their regular mesopore sizes (~3 nm), high surface areas (1300–2000 $m^2\ g^{-1}$), and high pore volumes (1–2 $cm^3\ g^{-1}$).[2–6] Vast progress has been made in the preparation of OMC materials with modified surfaces,[3] graphitic frameworks,[4] and pore structures,[5] which enable their utilization for various applications such as adsorbents, catalyst supports, nanotemplates, materials for advanced electronics, etc.[6] It is believed that a rational pathway for the synthesis of OMC materials with controlled pore sizes would greatly increase their suitability for some applications. Particularly OMC materials with large pore sizes are highly desirable for applications involving large molecules and fast mass transfer. However, while the pore size control of silica is comparatively successful, that of OMC materials is hitherto limited.[7]

Great efforts have been made to control the pore size of OMC materials, but only few successes have been reported in the literature yet, e.g., Ryoo and co-workers reported the synthesis of OMC materials with controllable pore sizes ranging from 2.2 to 3.3 nm using a mesoporous silica template with controlled silica wall thickness.[8] Syntheses of OMC materials with tuneable pore sizes using mesoporous silica templates with larger unit cell parameters while maintaining the regularity of mesopores have also been reported.[9] All of the trials reported, were based on the design of the starting mesoporous silica template, because the silica framework later generates the mesopores in the OMC material. The silica template needs to be designed appropriately in order to obtain OMC materials with controlled pore sizes, but in general, the pore size control of OMC materials, based on the design of a mesoporous silica template, has distinct limitations due to the difficult control of the properties of the silica framework.[10] Hence, different approaches were taken in order to satisfy the need for OMC materials with a controlled mesopore size, which yielded OMC materials with hierarchical porosity, e.g., bimodal mesoporous carbon materials constructed from nanopipes,[11] dual porous OMCs obtained via a dual templating route,[12] and hollow mesoporous carbon synthesized by chemical vapour deposition.[13].

Here we report for the first time, on a facial synthesis strategy for the production of OMC materials with systematically tuneable mesopore sizes in the range of 3–10 nm, where boric acid is utilized as a pore expanding agent (Scheme 1). As shown in Scheme 1, the difference between the proposed (A → D → E) and the conventional synthesis (A → B → C) route for OMC materials is the co-infiltration of boric acid together with the carbon precursor. A spontaneous phase separation of the boron species, which is present in the precursor-silica composite and contains sucrose and boric acid within the mesopores of a silica template, takes place during the carbonization process. This is expected to result in the subsequent formation of boron oxide and borosilicate nanolayers between the silica and carbon frameworks, which may result in an increased pore size for the OMC materials obtained, as shown in Scheme 1.

The present synthesis of OMC materials with controllable pore sizes uses a mixed aqueous solution of boric acid and sucrose (carbon precursor). A 2D hexagonal mesoporous silica, MSU-H, was synthesized following procedures reported elsewhere with slight modifications,[6g,14] and used as the silica template. After infiltration of the template by the precursor solution, followed by carbonization and removal of the silica template OMC materials with controlled pore sizes were obtained, herein referred to as OMC-B-*x*, where *x* denotes the mol% of boric acid in the precursor mixture. Obtained OMC-B-*x* materials exhibit a highly ordered 2D hexagonal mesostructure, similar to that of the mesoporous silica template, as

[*] Prof. Dr. J. M. Kim, Dr. H. I. Lee, J. H. Kim, J. E. Lee
Functional Materials Laboratory, Department of Chemistry, BK21 School of Chemical Materials Science, SKKU Advanced Institute of Nanotechnology and Research Institute of Advanced Nanomaterials, Sungkyunkwan University
Suwon 440-746 (Korea)
E-mail: jimankim@skku.edu
Dr. C. Pak, Dr. S. H. Joo, Dr. H. Chang, Dr. D. Seung, D. J. You
Energy and Environment Laboratory
Samsung Advanced Institute of Technology
PO Box 111, Suwon 440-600 (Korea)
E-mail: chanho.pak@samsung.com
Prof. Dr. W.-S. Ahn
Department of Chemical Engineering, Inha University
Incheon 402-751 (Korea)

[**] This work was supported by grant No. M102KP010015-07K1601-01512 from the Carbon Dioxide Reduction & Sequestration Center, one of the 21st Century Frontier Programs funded by the Ministry of Science and Technology of the Korean government. Supporting Information is available online from Wiley InterScience or from the author.

ADVANCED MATERIALS

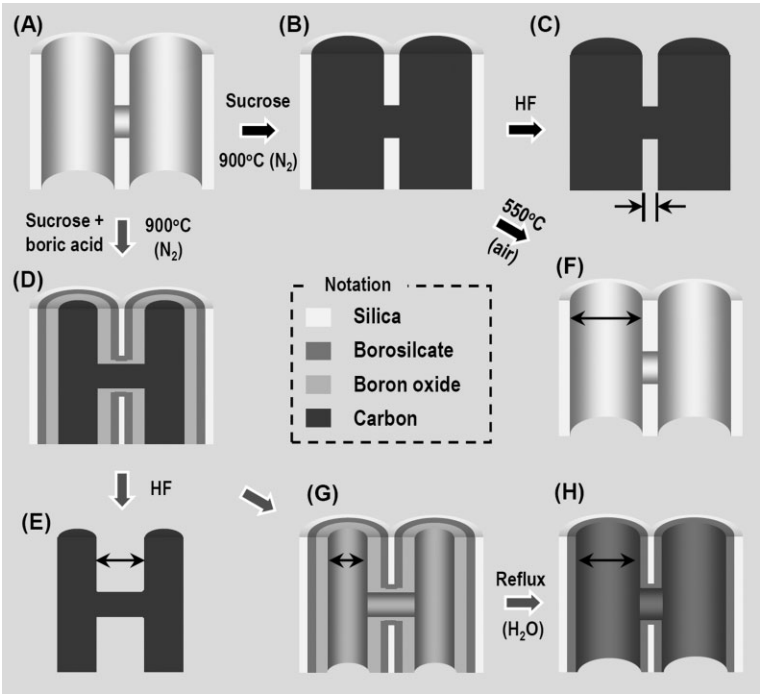

Scheme 1. Schematic illustration of pore expansion mechanism and conventional route for the synthesis of ordered mesoporous carbon (OMC). A) Mesoporous silica template. B) Silica/carbon composite. C) Conventional OMC material obtained by removal of the silica template from B) using HF. D) Silica/borosilicate/boron oxide/carbon composite. E) Larger porous OMC material obtained by removal of the silica template using HF. F) Mesoporous silica prepared by calcining B) in ambient conditions. G) Mesoporous silica/borosilicate/boron oxide composite prepared by calcination of D) in ambient conditions. H) Mesoporous silica/borosilicate composite obtained after removal of boron oxide from G) by refluxing with deionized water.

can be seen from the X-ray diffraction (XRD) patterns shown in Figure 1A. The XRD patterns exhibit well resolved peaks corresponding to the 100, 110, and 200 planes. And as shown in Figure 1A and Table 1, no significant changes in the XRD pattern and the unit cell parameter (a_0) were observed when the amount of boron species was increased to 25 mol%. Figures 1B and 1C show N_2 adsorption-desorption isotherms and the corresponding pore size distribution curves (BJH method), respectively, for various OMC-B-*x* materials synthesized. As can be seen from Figure 1B, all N_2 sorption isotherms are type IV isotherms with hysteresis loops, which corresponds to data reported elsewhere.[1–6] Well defined steps appear in the adsorption-desorption curves at a relative pressure, p/p_0, of 0.4 to 0.9, depending on the boron content of the precursor solution. In the case of OMC-B-0, N_2 adsorption rapidly increases at specific relative pressures of $p/p_0 = 0.45 - 0.55$, due to capillary condensation within the mesopores. Remarkably, the position of the sharp step in the isotherm gradually shifts to higher relative pressures as the boron content increases, indicating that there is a systematic increase in mesopore size which is proportional to the boron content (Fig. 1B). The deviation in mesostructural properties such as unit cell parameter, pore volume, pore diameter, and surface area with increasing boron content is summarized in Table 1. BJH pore size distribution curves displayed in Figure 1C clearly show the shift of the average diameter of mesopores from 3.8 nm to 4.9, 5.5, 6.4, 8.5, and 10.0 nm, respectively, without significant widening of the size distribution (except for OMC-B-25) and loss of mesostructural order, as previously concluded from the XRD data shown in Figure 1A. Compared with other OMC-B-*x* materials, OMC-B-25 exhibits a much broader pore size distribution centered on 10.5 nm, which may be due to some structural breakdown.

Table 1. Physical properties of OMC-B-*x* materials and mesoporous silica template.

Samples	a_0 [nm] [a]	D_p [nm] [b]	V_{tot} [cm^3/g] [c]	$V_{<2\ nm}$ [cm^3/g] [d]	S_{BET} [m^2/g] [e]
OMC-B-0	11.7	3.8	1.60	0.56	1337
OMC-B-2	11.5	4.9	1.35	0.51	1214
OMC-B-4	11.5	5.5	1.25	0.45	1049
OMC-B-8	11.5	6.4	1.20	0.38	898
OMC-B-12	11.7	8.5	1.19	0.37	860
OMC-B-16	11.7	10.0	1.43	0.39	912
OMC-B-25	11.7	10.5	1.25	0.36	848
MSU-H	13.2	12.0	1.17	–	440

[a] Unit cell parameters calculated from XRD data using the equation $a_0 = d_{100}$ X (2/v3). [b] Mesopore diameters calculated from the N_2 adsorption branches using the BJH method. [c] Total pore volumes estimated from the N_2 sorption isotherms at $p/p_0 = 0.99$. [d] Pore volume of pores with diameters less than 2 nm calculated at $p/p_0 = 0.16$ using the Horvath-Kawazoe formula. [e] Surface areas calculated using the BET method.

Figure 2 shows Field-emission scanning electron microscopy (FE-SEM) and transmission electron microscopy (TEM) images of various OMC-B-*x* materials. FE-SEM images shown in Figures 2A – 2D reveal that the morphology of OMC-B-*x* materials, which is similar to the one observed for the mesoporous silica template, is maintained at different amounts of boric acid in the precursor solution. FE-SEM analysis of OMC-B-16 using a higher magnification indicates that the material consists of very fine carbon nanorods with expanded mesopores between single rods (Fig. 2D). Pore structures can be seen more clearly in the TEM images shown in Figures 2E – 2H. The size of mesopores gradually increases with the amount of boric acid in the precursor solution without significant loss of mesostructural order. These findings are in good agreement with the XRD and N_2 sorption data shown in Figure 1. TEM images also indicate that the diameter of carbon rods decreases with an increasing boron content, thereby causing the apparent expansion of the mesopores. Quite reasonably this is the result of an increased degree of packing of carbon species within the framework which originates from a decreased mesopore size of the silica template

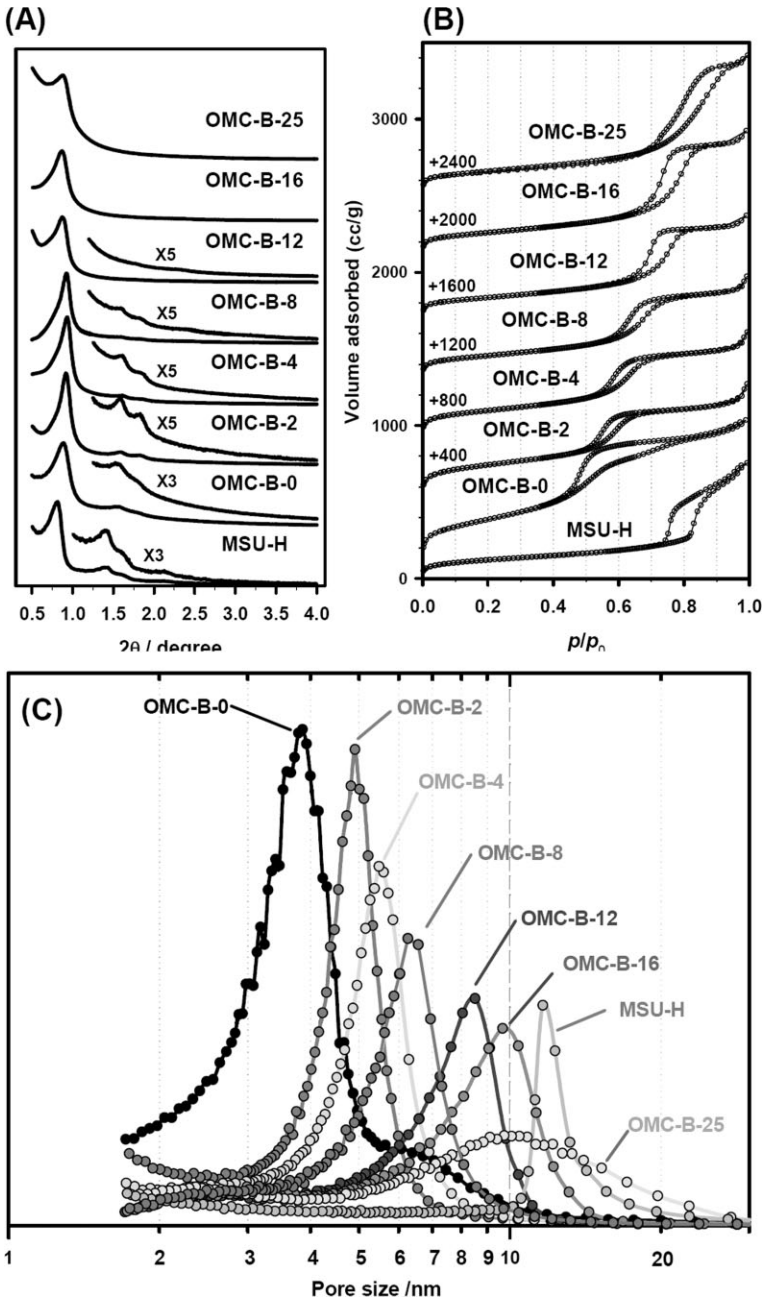

Figure 1. A) X-ray diffraction (XRD) patterns, B) N_2 adsorption-desorption isotherms, and C) corresponding pore size distribution curves for the mesoporous silica template (MSU-H) and all OMC-B-*x* materials obtained. Pore size distribution curves were calculated from adsorption branches using the BJH method.

due to nanolayer coating during the carbonization, hence limited volumes for the formation of the carbon framework and thus a more dense packing. This explanation is in good agreement with the decreasing pore volume observed for pores that are smaller than 2 nm in size (Table 1).

The pore expansion mechanism for the synthesis of OMC materials with controllable mesopore sizes (A → D → E route in Scheme 1) has been investigated by a combination of characterization techniques including Fourier transform infrared spectroscopy (FT-IR), ^{11}B magic angle spinning (MAS) NMR, and N_2 sorption. Figure 3 shows the FT-IR spectra collected after each step of the preparation of OMC-B-8. As described in the experimental section, OMC-B-*x* materials are obtained by infiltrating a silica template with a mixture of carbon precursor and boric acid, followed by aging of the composite at 160 °C, and carbonization at 900 °C. As shown in Figure 3, there is no significant difference in the FT-IR spectra observed until the carbonization temperature reaches 400 °C. The composite samples, after both, drying at 160 °C and carbonizing at 400 °C, only exhibit IR bands corresponding to B–O (~1450 and ~1200 cm^{-1}) and Si–O bonds (~1080, ~800, and ~460 cm^{-1}).[15] When the carbonization temperature rises to 650 °C, additional bands appear at ~920 and ~670 cm^{-1}, indicating the formation of Si–O–B linkages. The intensity of these bands increases as the carbonization temperature increases. The formation of a rigid carbon framework from sucrose starts at roughly 600 °C during the carbonization process for the synthesis of OMC materials.[16] Therefore, it is reasonable to believe that the boron species in the mixture of sucrose and boric acid is first transformed into boron oxide within the mesoporous silica template, before undergoing a spontaneous phase separation and moving from the boron-carbon mixture to the silica surface as the temperature increases, and finally reacting with the silica framework which produces a borosilicate layer.

The formation of borosilicate during the synthesis of OMC-B-*x* materials was also confirmed by ^{11}B MAS NMR spectroscopy (Fig. S1 in Supporting Information). Prior to the removal of the inorganic template, the silica/boron/carbon composite material (sample D in Scheme 1) exhibits broad NMR peaks at 9 and -2.5 ppm, which correspond to trigonal BO_3 and tetrahedrally coordinated boron groups, respectively. This result indicates that borosiloxane bonds (=B-O-Si=) are present and that some boron atoms show tetrahedral coordination to -O-Si groups.[17] These NMR peaks become more resolved in the silica/borosilicate/boron oxide composite material after the removal of carbon (sample G in Scheme 1), as shown in Figure S1.

Figure 4 shows XRD patterns and N_2 sorption data for samples corresponding to stages F, G, and H in Scheme 1 (boron content: 8 mol%), which were collected in order to investigate presence as well as thickness of the borosilicate and boron oxide layers on the surface of the mesoporous silica template. Samples F and G were obtained via calcination of samples B and D in air at 550 °C in order to remove the carbon frameworks from the silica/carbon composite and silica/boron/car-

ADVANCED MATERIALS

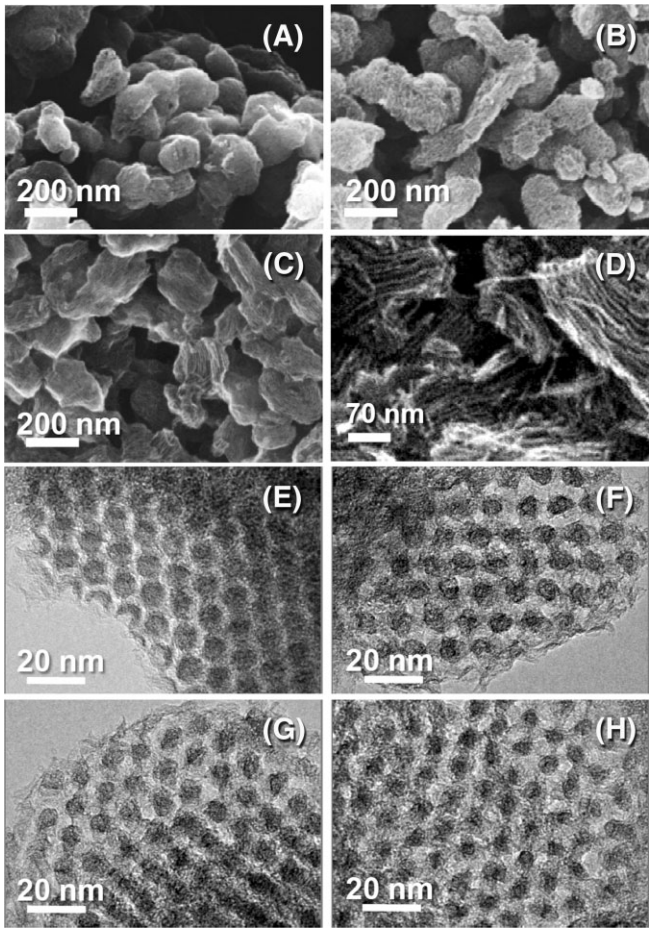

Figure 2. Field-emission scanning electron microscopy (FE-SEM) images of A) OMC-B-0, B) OMC-B-8, C) OMC-B-16, and D) OMC-B-16 in higher magnification. Transmission electron microscopy (TEM) images of E) OMC-B-0, F) OMC-B-8, G) OMC-B-12, and H) OMC-B-16.

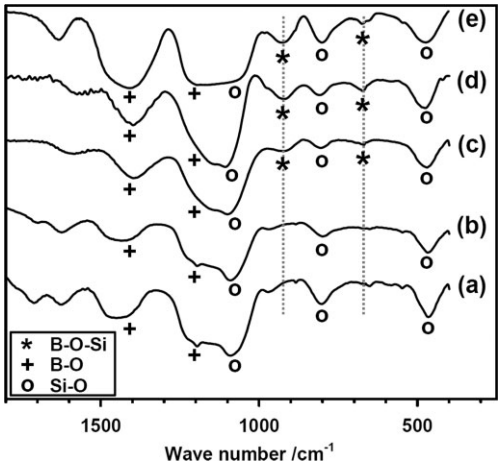

Figure 3. Fourier transform infrared (FT-IR) spectra collected at each preparation step of OMC-B-8. (a) Silica/boron/carbon composite dried at 160 °C. (b)-(d) Composite material after heattreatment at 400 °C, 650 °C and 900 °C, respectively, under N2 flow. (e) Silica/boron composite after removal of the carbon framework by calcination (sample G in Scheme 1).

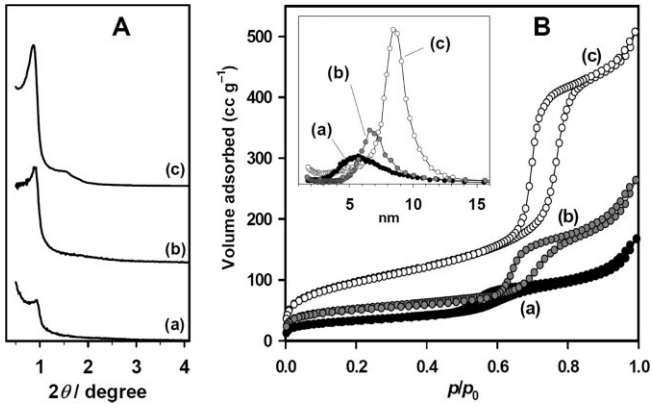

Figure 4. A) XRD patterns and B) N_2 adsorption-desorption isotherms and corresponding BJH pore size distribution curves (inset) for (a) Mesoporous silica/borosilicate/boron oxide composites (sample G in scheme 1), (b) Mesoporous silica/borosilicate composites (sample H in scheme 1), and (c) Mesoporous silica (sample F in scheme 1).

bon composite, respectively. Sample H was prepared by refluxing sample G in boiling water for 6 h, which selectively removed boron oxide species from the silica/boron composite. Even though, minor losses in the mesoscopic long-range order were observed when comparing the samples to the parent mesoporous silica template (MSU-H, Fig. 1A), all three samples exhibited similar XRD peaks at low angles, and their lattice parameters ($a_0 = 12.0$ nm) are similar to that of OMC-B-8. N_2 sorption isotherms and corresponding BJH pore size distribution data show that the samples F, G, and H exhibit mesopores with sizes of 8.5, 5.5, and 6.9 nm, respectively (Fig. 4). Therefore, according to the lattice parameters and pore size results shown, the framework thickness of the mesoporous silica/boron composite (~6.5 nm, sample G) is larger than that of the mesoporous silica (~3.5 nm, sample F). The increased framework thickness is probably due to the formation of borosilicate and boron oxide layers on the silica surface, as verified by previously discussed FT-IR and ^{11}B MAS NMR results. Moreover the enlarged framework thickness (~3 nm) of the silica/boron composite (sample G) is in close agreement with the pore size expansion of OMC-B-8 (6.4 nm) compared to OMC-B-0 (3.8 nm), because the removal of the inorganic framework results in mesoporous OMC materials.[1–6] A comparison of pore sizes between samples G and H indicates that the enlarged inorganic framework consists of silica, borosilicate and boron oxide, and that the thickness of the boron oxide layer is about 1.4 nm. Based on the FT-IR, ^{11}B MAS NMR, and N_2 sorption results, the pore expansion of OMC materials caused by additional boron species in the carbon precursors is probably due to a spontaneous phase separation of boron species and carbon precursor within the mesopores of the silica template and subsequent solid state reaction between silica framework and boron species during the carbonization process (A → D → E route in Scheme 1).

In conclusion, we report on a novel synthesis pathway for the preparation of OMC materials with precisely controllable

pore sizes in the range of 3–10 nm using boric acid as the pore expanding agent while the mesopore structure is retained. In particular, the pore expansion mechanism, involving a spontaneous phase separation of the boron species from the mixture of boron and carbon precursors to the silica surface of mesoporous silica template was investigated. OMC materials with tuneable pore sizes are expected to be highly beneficial for various practical applications, such as catalysis, adsorption, separation, energy conversion, etc. The present synthesis pathway using an inorganic pore expanding agent is expected to be a facile and general method for the pore size control of various types of mesostructured carbon materials. The effects of other inorganic species on the formation and structural properties of OMC materials are also under investigation and will be reported in due course.

Experimental

Synthesis of ordered mesoporous silica template: A mesoporous silica template (MSU-H) exhibiting a 2D-hexagonal structure was synthesized following procedures described elsewhere with slight modifications [6g, 14]. Briefly, a sodium silicate solution (SiO_2 = 10 wt%, Na/Si = 2.5) was prepared by dissolving Ludox-HS40 (Aldrich) in an aqueous solution of NaOH at 80 °C and subsequent cooling to room temperature. The sodium silicate solution was then added to an aqueous solution of P123 ($EO_{20}PO_{70}EO_{20}$, MW = 5800 g·mol^{-1}, Aldrich) at 25 °C. After stirring for 10 min acetic acid, in an amount equivalent to the amount of sodium hydroxide in the silicate solution, was poured into the mixture for neutralization (pH ~ 7.0). Following further stirring for 10 min, the mixture was heated to 45 °C and subsequently stirred at this temperature for 24 h. The overall molar composition of the mixture was 1.00 SiO_2 : 2.5 NaOH : 2.5 acetic acid : 0.017 P123 : 230 H_2O. The reaction vessel was then heated to 100 °C and kept at this temperature for 24 h under static conditions in an oven. The solid product was filtered, washed with water, and dried in air before being calcined in air at 550 °C.

Synthesis of ordered mesoporous carbon: The procedure for the synthesis of ordered mesoporous carbon (OMC) materials is the same as the nano-replication method described elsewhere [1–6], except for the use of a mixture of sucrose and boric acid as the precursor solution. The boric acid content in the precursor solutions was in the range of 0–25 mol% (boric acid/(boric acid + sucrose)). Precursor solutions were prepared by adding various amounts of boric acid to a sucrose solution whereby the sucrose concentration was kept constant. OMC materials obtained were denoted as OMC-B-*x*, where *x* stands for the molar fraction of boron. A typical procedure for, e.g., the preparation of OMC-B-8 can be described as follows: a precursor solution, containing boric acid (0.226 g), sulfuric acid (0.141 g), sucrose (1.25 g), and distilled water (4.0 mL) was allowed to infiltrate the mesopores of the silica template. The composite material was then dried at 100 °C for 6 h and at 160 °C for 6 h thereafter. The infiltration and drying process were repeated once more with additional 3.66 g of precursor solution (66 % of first infiltration), before the composite was carbonized at 900 °C for 3 h under N_2 flow. Finally, the OMC-B-8 material was obtained by removal of the inorganic framework using an HF solution.

Characterization: Small-angle X-ray diffraction (XRD) patterns were obtained using a synchrotron X-ray source, BL8C2, at the Pohang Light Source facility (reflection mode, λ = 0.154250 nm). N_2 adsorption-desorption isotherms were collected on a Micromeritics ASAP 2010 system at liquid N_2 temperature. All samples were degassed at 200 °C prior to N_2 sorption analysis. Field-emission scanning electron micrographs (FE-SEM) were obtained with a LEO SUPRA 55 GENESIS 2000 instrument, operating at an accelerating voltage of 15 kV. Transmission electron microscopy (TEM) images were collected using a G2 FE-TEM, operating at 200 kV. IR spectra were collected on a Bruker TENSOR27, and ^{11}B MAS NMR spectra were obtained with a Bruker AVANCE 400 WB DSX-400 spectrometer operating at 128.5 MHz. Chemical shifts were referenced to $BF_3O(CH_2CH_3)_2$.

Received: September 1, 2007
Revised: November 21, 2007
Published online: January 29, 2008

[1] a) R. Ryoo, S. H. Joo, S. Jun, *J. Phys. Chem. B* **1999**, *103*, 7743. b) J. Lee, S. Yoon, T. Hyeon, S. M. Oh, K. B. Kim, *Chem. Commun.* **1999**, 2177.

[2] J. Lee, J. Kim, T. Hyeon, *Adv. Mater.* **2006**, *18*, 2073.

[3] a) H. Darmstadt, C. Roy, S. Kaliaguine, S. J. Choi, R. Ryoo, *Carbon* **2002**, *40*, 2673. b) D. J. Kim, H. I. Lee, J. E. Yie, S. J. Kim, J. M. Kim, *Carbon* **2005**, *43*, 1868.

[4] a) T. W. Kim, I. S. Park, R. Ryoo, *Angew. Chem. Int. Ed.* **2003**, *42*, 4375-7379. b) A. B. Fuertes, S. Alvarez, *Carbon* **2004**, *42*, 3049. c) C. H. Kim, D.-K. Lee, T. J. Pinnavaia, *Langmuir* **2004**, *20*, 5157.

[5] a) S. H. Joo, S. Jun, R. Ryoo, *Micropor. Mesopor. Mater.* **2001**, *44*, 153. b) S. Jun, S. H. Joo, R. Ryoo, M. Kruk, M. Jaroniec, Z. Liu, T. Oshuna, O. Terasaki, *J. Am. Chem. Soc.* **2000**, *122*, 10712. c) R. Ryoo, S. H. Joo, M. Kruk, M. Jaroniec, *Adv. Mater.* **2001**, *13*, 677. d) Y. Sakamoto, T.-W. Kim, R. Ryoo, O. Terasaki, *Angew. Chem. Int. Ed.* **2004**, *43*, 5231.

[6] a) S. Y. Park, B. H. Choi, M. Kang, J. M. Kim, I. M. Lee, *J. Mol. Catal. A* **2007**, *265*, 323. b) S. Y. Lim, M. Kang, J. M. Kim, I. M. Lee, *Bull. Korean Chem. Soc.* **2005**, *26*, 887. c) S. Y. Park, M. Kang, J. E. Yie, J. M. Kim, I. M. Lee, *Tetrahedron Lett.* **2005**, *46*, 2849. d) Y. Jung, J. W. Yeon, J. M. Kim, H. I. Lee, S. Kim, S. J. Park, *Solid State Phenomena* **2007**, *124-126*, 1781. e) Y. Jung, S. Kim, S. J. Park, J. M. Kim, *Coll. Surf. A* **2007**, in press. f) M. Choi, R. Ryoo, *Nature Mater.* **2003**, *2*, 473. g) S. H. Joo, C. Pak, D. J. You, S. -A. Lee, H. I. Lee, J. M. Kim, H. Chang, D. Seung, *Electrochim. Acta* **2006**, *52*, 1618. h) M. Kang, S. H. Yi, H. I. Lee, J. E. Yie, J. M. Kim, *Chem. Commun.* **2002**, 1944. i) A.-H. Lu, W. Schmidt, A. Taguchi, B. Spliethoff, B. Tesche, F. Schüth, *Angew. Chem. Int. Ed.* **2002**, *41*, 3489. j) A.-H. Lu, F. Schüth, *Adv. Mater.* **2006**, *18*, 1793. k) H. Chang, S. H. Joo, C. Pak, *J. Mater. Chem.* **2007**, *17*, 3078.

[7] a) C. T. Kresge, M. E. Leonowicz, W. J. Roth, J. C. Vartuli, J. S. Beck, *Nature* **1992**, *359*, 710. b) D. Zhao, J. Feng, Q. Huo, N. Melosh, G. H. Fredrickson, B. F. Chmelka, G. D. Stucky, *Science* **1998**, *279*, 548. c) J. S. Lettow, Y. J. Han, P. Schmidt-Winkel, P. Yang, D. Zhao, G. D. Stucky, J. Y. Ying, *Langmuir* **2000**, *16*, 8291. d) S. S. Kim, A. Karkamkar, T. J. Pinnavaia, M. Kruk, M. Jaroniec, *J. Phys. Chem. B* **2001**, *105*, 7663.

[8] J. S. Lee, S. H. Joo, R. Ryoo, *J. Am. Chem. Soc.* **2002**, *124*, 1156.

[9] a) C. Yu, J. Fan, B. Tian, D. Zhao, G. D. Stucky, *Adv. Mater.* **2002**, *14*, 1742. b) A. B. Fuertes, *Micropor. Mesopor. Mater.* **2004**, *67*, 273. c) S. Alvarez, A. B. Fuertes, *Carbon* **2004**, *42*, 433. d) A. Vinu, C. Streb, V. Murugesan, M. Hartmann, *J. Phys. Chem. B* **2003**, *107*, 8297. e) Y. Xia, Z. Yang, R. Mokaya, *Chem. Mater.* **2006**, *18*, 140.

[10] a) A. Sayari, P. Liu, M. Kruk, M. Jaroniec, *Chem. Mater.* **1997**, *9*, 2499. b) R. Mokaya, *J. Phys. Chem. B* **1999**, *103*, 10204.

[11] a) S. H. Joo, S. J. Choi, I. Oh, J. Kwak, Z. Liu, O. Terasaki, R. Ryoo, *Nature* **2001**, *412*, 169. b) A.-H. Lu, W.-C. Li, W. Schmidt, F. Schüth, *Micropor. Mesopor. Mater.* **2005**, *80*, 117.

[12] a) H. I. Lee, C. Pak, C. H. Shin, H. Chang, D. Seung, J. E. Yie, J. M. Kim, *Chem. Commun.* **2005**, 6035. b) Y. Deng, C. Liu, T. Yu, F. Liu, F. Zhang, Y. Wan, L. Zhang, C. Wang, B. Tu, P. A. Webley, H. Wang,

D. Zhao, *Chem. Mater.* **2007**, *19*, 3271. c) J. Lee, K. Sohn, T. Hyeon, *J. Am. Chem. Soc.* **2001**, *123*, 5146. d) J. Lee, J. Kim, T. Hyeon, *Chem. Commun.* **2003**, 1138. e) S. B. Yoon, K. Sohn, J. Y. Kim, C. H. Shin, J. S. Yu, T. Hyeon, *Adv. Mater.* **2002**, *14*, 19.

[13] Y. Xia, R. Mokaya, *Adv. Mater.* **2004**, *16*, 886.

[14] S.-S. Kim, T.R. Pauly, T. J. Pinnavaia, *Chem. Commun.* **2000**, 1661.

[15] M. A. Beckett, M. P. Rugen-Hankey, K. S. Varma, *Chem. Commun.* **2000**, 1499.

[16] a) D. J. Kim, H. I. Lee, J. E. Yie, S. J. Kim, J. M. Kim, *Carbon* **2005**, *43*, 1868. b) H. I. Lee, J. H. Kim, S. H. Joo, H. Chang, D. Seung, O. S. Joo, D. J. Suh, W. S. Ahn, C. Pak, J. M. Kim, *Carbon*, **2007**, in press.

[17] a) A. D. Irwin, J. S. Holmgren, J. Jonas, *J. Non-Cryst. Solids* **1988**, *101*, 249. b) I. Eswaramoorthi, A. K. Dalai, *Micropor. Mesopor. Mater.* **2006**, *93*, 1. c) T. P. Xiu, Q. Liu, J. C. Wang, *J. Mater. Chem.* **2006**, *16*, 4022.

